



SOC estimation for lithium-ion battery using the LSTM-RNN with extended input and constrained output[☆]

Junxiong Chen, Yu Zhang, Ji Wu, Weisong Cheng, Qiao Zhu^{*}

School of Mechanical Engineering, Southwest Jiaotong University, Chengdu, 610031, China

ARTICLE INFO

Keywords:

State of charge estimation
LiFePO₄ battery
Long short-term memory
Recurrent neural network
Extended input
Constrained output

ABSTRACT

The state of charge (SOC) estimation of lithium-ion battery (LIB) based on recurrent neural network (RNN) has been a popular research due to its suitability for time series data prediction. However, there are significant output fluctuations in solo network, which lead to unstable SOC estimation performance. To solve this problem, this paper proposes a novel long short-term memory recurrent neural network (LSTM-RNN) with extended input (EI) and constrained output (CO) for battery SOC estimation, named EI-LSTM-CO. For the network input, an additional slow time-varying information sliding window average voltage is introduced to enhance the ability of network to map the nonlinear characteristics of the battery and reduce the output SOC fluctuations. In terms of the network output, a state flow strategy based on the Ampere-hour integration (AhI) is designed to constrain the variation between adjacent output SOCs of the network to smooth the network output and further improve the SOC estimation performance. In the experiments, the LiFePO₄ battery datasets at various temperatures are used to validate the SOC estimation performance and generalization ability. In particular, the root mean square error (RMSE) and the maximum error (MAXE) of the proposed method on unknown data are less than 1.3% and 3.2% respectively.

1. Introduction

As the fastest developing and most promising energy storage device, lithium-ion battery (LIB) have attracted extensive attention in the field of electric vehicle (EV) due to its high energy density, fast charging, long service life, low memory effect, low self-discharge rate, and low pollution [1]. The battery state of charge (SOC) is one of the key states that need to be monitored in battery applications and plays a crucial role in the safe and rational use of battery. The battery SOC is defined as the percentage of the remaining available capacity relative to the nominal capacity [2], which is an estimated parameter rather than an observable parameter, so it cannot be obtained directly by sensor measurement, but needs to be estimated indirectly by the battery management system (BMS) using relevant algorithms. Due to the highly nonlinear nature of the LIB itself and the constantly changing operating conditions, it is still a challenging task to accurately estimate battery SOC in real time [3].

1.1. Literature review

So far, researchers have done a lot of research and made significant progress in battery SOC estimation. In this paper, existing SOC estimation methods are classified into the following categories based on the principle and application nature of the method: definition method [4,5], direct method [6–23], indirect method [24–44], and calibration method [45,46].

1.1.1. Defined method

The definition method is the Ampere-hour integration (AhI) method, whose estimation principle is the Coulomb counting [4], and it is the most accurate method for battery SOC estimation theoretically. However, the AhI method has two obvious drawbacks that affect the accuracy of SOC estimation in practice. One is the accumulated error of the Coulomb counting for a long time due to the bias of current sampling, and the other is the high dependence on the accurate initial

[☆] This work is partially supported by the National Natural Science Foundation of China (No. 51775450) and the Sichuan Science and Technology Program (No. 2022YFG0094 and 2019JDRC0025).

* Corresponding author.

E-mail addresses: cjxlm@my.swjtu.edu.cn (J. Chen), lioyzhnagy@163.com (Y. Zhang), wuji@my.swjtu.edu.cn (J. Wu), weisongCC@my.swjtu.edu.cn (W. Cheng), zhuqiao@home.swjtu.edu.cn (Q. Zhu).

Nomenclature	
ACDKF	Adaptive central difference Kalman filter
ACKF	Adaptive cubature Kalman filter
AE	Autoencoder
AhI	Ampere-hour integration
AHIF	Adaptive H-infinity filter
APF	Adaptive particle filter
BMS	Battery management system
BPNN	Back propagation neural network
CALCE	Center for Advanced Life Cycle Engineering
CO	Constrained output
DAE	Denoising autoencoder
DEKF	Dual extended Kalman filter
DNN	Deep neural network
DP	Dual-polarization
DST	Dynamic stress testing
ECM	Equivalent circuit model
EI	Extended input
EKF	Extended Kalman filter
EM	Electrochemical model
EV	Electric vehicle
FFNN	Feedforward neural network
FNTSMO	Fast non-singular terminal sliding mode observer
FO	Fractional-order
FUDS	Federal urban driving schedule
GPR	Gaussian process regression
GRU	Gated recurrent unit
HIF	H-infinity filter
IBGRU	Improved bidirectional gated recurrent unit
IFO	Improved fractional-order
IHF	Improved H-infinity filter
IIO	Innovative immersion and invariance adaptive observer
ISRCKF	Improved square root-cubature Kalman filter
KF	Kalman filter
LIB	Lithium-ion battery
LSSVM	Least square support vector machine
LSTM	long short-term memory
MAXE	Maximum error
ML	Machine learning
MSE	Mean square error
NN	Neural network
OCV	Open-circuit voltage
P2D	Pseudo-two-dimensional
PBM	Physics-based battery model
PF	Particle filter
PSO	Particle swarm optimization
RBFNN	Radial basis function neural network
RMSE	Root mean square error
RNN	Recurrent neural network
SFNN	Stochastic fuzzy neural network
SOC	State of charge
SVM	Support vector machine
TM	Thevenin mode
TORC	Second-order RC
UKF	Unscented Kalman filter
UPF	Unscented particle filter
USABC	United States Advanced Battery Consortium

categories depending on the type of model: linear model-based method [6] and machine learning (ML) model-based method [7–23]. The linear model-based method refers to the battery open-circuit voltage (OCV) method [6]. The OCV method uses the monotonic OCV-SOC relation to look up tables and interpolate to obtain the SOC. However, in order to obtain a stable OCV, the battery needs to be left to rest for more than 2 h, which limits the online application of the OCV method. The ML model-based method establishes the direct nonlinear mapping between the battery measured variables and SOC through off-line learning of battery dynamic operating data, without the need for accurate formulas or models, so it has attracted wide attention in recent years [7]. Examples include support vector machine (SVM) [8], Gaussian process regression (GPR) [9], back propagation neural network (BPNN) [10], and radial basis function neural network (RBFNN) [11], etc. Because SOC estimation is essentially a prediction problem for time series data, the recurrent neural network (RNN) with historical information processing abilities has become popular for research [12,13]. And since the RNN cannot capture the long-term dependencies, the long-short term memory (LSTM) [14–17] and the gated recurrent unit (GRU) [18–21] with gating mechanisms are proposed to improve the RNN. Ren et al. [14] optimized the key parameters of LSTM-RNN by using the particle swarm optimization (PSO) algorithm to improve the SOC estimation accuracy, and added the random noise to the input layer of the network during training process in order to improve the anti-interference ability of the network. Jiao et al. [18] investigated a GRU-RNN based momentum gradient method and analyzed the influences of the momentum terms, noise variances, training epochs, and number of hidden layer neurons on the training speed and SOC estimation accuracy of the network. In addition, Fasahat et al. [22] and Chen et al. [23] investigated the combinational network by connecting the autoencoder (AE) in series with the RNN, and used the AE to extract useful data features from the battery measured variables, which helps the RNN to learn the battery nonlinear mapping rule. Since the ML model-based method uses the direct mapping for SOC estimation, each calculation of SOC is independent rather than iterative, so there is neither accumulated error nor dependence on accurate initial SOC. However, because of this, the output SOC of the ML model-based method has significant fluctuations when the battery voltage and current change drastically, and this problem cannot be solved by tuning the network hyperparameters, which greatly affects the stability and accuracy of SOC estimation.

1.1.3. Indirect method

The indirect method takes the AhI method as the main calculation part for SOC estimation, combines the battery model and then use the filter or observer to assist in correcting the SOC to solve the two defects in the solo AhI method. According to the model types and modeling objects, it can be divided into four categories: the electrochemical model (EM)-based voltage correction method [24–26], the equivalent circuit model (ECM)-based voltage correction method [27–34], the ML model-based voltage correction method [35–37], and the ML model-based SOC

SOC [5]. Therefore, to solve these two problems, a large number of battery SOC estimation methods have been investigated.

1.1.2. Direct method

The direct method is to map the SOC directly using the battery measured variables (voltage, current, temperature and impedance) with the help of the established battery characteristic model. There are two

correction method [38–44]. The EM-based voltage correction method describes the battery dynamic characteristics using the mathematical equations according to the internal mechanism of the battery. However, due to the difficulty of calculation, this method is difficult to estimate online, so it is not suitable for practical application. The ECM-based voltage correction method is the most studied one at present. Firstly, a priori SOC is estimated by the AhI method, and then the priori SOC is combined with the ECM to calculate the battery model terminal voltage [27]. The error between the measured terminal voltage and the model terminal voltage is utilized to correct the prior SOC according to the gain parameter of the filter algorithm, thus the final estimated SOC is obtained. There are many types of filters available, such as the Kalman filter (KF) [28–30], H-infinity filter (HIF) [31,32], particle filter (PF) [33], and sliding mode observer [34]. However, the ECM-based voltage correction method is highly dependent on the accurate battery model, and due to the complex dynamic characteristics of the battery, and the influence of temperature and aging, especially the OCV of some batteries is not sensitive with SOC varying, which makes it difficult to obtain an accurate battery ECM in the practical application, hence this method cannot provide appropriate SOC correction for the AhI method in many cases. Besides, Charkhgard et al. [35–37] used the ML model to play the role of the ECM for establishing the mapping relation from the battery SOC to the terminal voltage, thus this class of methods has the same drawbacks as the ECM-based voltage correction method. In addition to building the battery voltage model to correct the AhI method, the researchers tried to establish the battery SOC mapping model directly using the ML method, to make the SOC become an observation signal and the error between the prior SOC and the observed SOC can be used to correct the SOC of the AhI method. He et al. [38] pioneered this method by establishing the state function based on the AhI method, establishing the battery SOC observation function based on the neural network (NN), and using the UKF for information fusion to complete the stable estimation of SOC. Considering the lack of time series data processing ability of the simple NN, Yang et al. [39–41] established the mapping of battery measured variables to SOC based on the LSTM-RNN, and the unscented Kalman filter (UKF), adaptive cubature Kalman filter (ACKF) and adaptive H-infinity filter (AHIF) were used for SOC estimation respectively. Similarly, Cui et al. [42] combined the improved bidirectional gated recurrent unit (IBGRU) and UKF for SOC estimation. In addition, Song et al. [43] fused the output SOC of the least square support vector machine (LSSVM) with the SOC from AhI method by using the unscented particle filter (UPF). Shen et al. [44] modeled the battery SOC mapping by using a transformer NN and used an innovative immersion and invariance adaptive observer (IIO) to reduce the fluctuations in the network output SOC. Compared with the battery voltage model, the battery SOC model is much less influenced by the OCV-SOC plateau, so the ML model-based SOC correction method has lower requirements on the accuracy of the observation signal, lower computational complexity, and better SOC estimation performance.

1.1.4. Calibration method

In addition to the above methods for SOC estimation during battery operation, there are articles dedicated to the calibration of SOC during battery charging. Tian et al. [45] combined a deep neural network (DNN) with the standard KF to calibrate the initial SOC of the AhI method by using the charging data of voltage and current within 10 min. Based on the latest five charging protocols, Hu et al. [46] investigated a DNN using the battery charging data to estimate the SOC during charging as the initial SOC of the AhI method in the discharge process, and verified that the method has good robustness at different temperatures in the experiments.

1.2. Motivation

Table 1 summarizes the characteristics of the above four methods, including the SOC accumulated error, initial SOC dependence, SOC estimation accuracy, method complexity and practicality. It can be seen from the table that the ML model-based method, the ML model-based SOC correction method and the calibration method have the highest practicability. As the calibration method is outside the scope of this study, it will not be discussed too much in this paper. Compared with the ML model-based method, the ML model-based SOC correction method is more accurate, but it has higher complexity because it is a combined method. And the adaptive algorithm introduced into the filter and observer for adapting to the time-varying measurement noise of the battery will greatly increase the calculation amount of the method because of the sliding window covariance calculation. In contrast, if the fluctuations of the output SOC can be reduced by processing the input and output information of the ML model, then the ML model-based method would be more suitable for engineering application.

1.3. Key contributions

Aiming at the problem that the output SOC of the existing ML model-based methods fluctuates greatly, this paper improves the input and output information of the model respectively, and proposes a novel LSTM-RNN with extended input (EI) and constrained output (CO) for battery SOC estimation, named EI-LSTM-CO. The purpose of this study is to further improve the SOC estimation performance of the ML model-based methods [14,18,39,40]. The main contributions are as follows:

- (1) To address the problem of the significant output SOC fluctuations brought by the direct mapping using fast time-varying input information such as battery measured voltage, current, and temperature, this paper introduces an additional sliding window average voltage as slow time-varying information at the input of LSTM-RNN, to help learn the mapping related to the internal characteristics of battery when the battery voltage and current change rapidly, and reduce the fluctuations of the network output SOC. The experimental results show the validity of this behavior.
- (2) An AhI-based state flow strategy is designed at the output of LSTM-RNN to constrain the variation between adjacent output SOCs and achieve the effect of smoothing the network output SOC. The validity of this method is experimentally demonstrated. Compared with the existing filter-based smoothing methods, the proposed state flow constraint strategy is simpler and more effective, and has higher computation efficiency while ensuring the smoothing performance.
- (3) The experimental comparison with the methods using the same public dataset proves that the proposed method has outstanding performance in SOC estimation. Moreover, this method is still based on the direct mapping of ML for estimation, thus the BMS can start the calculation process without setting an accurate initial SOC.

1.4. Organization of the paper

The remainder of this paper is organized as follows: Section 2 describes the principle of the proposed SOC estimation method in detail. Section 3 introduces the battery dataset and the evaluation criteria used in the experiments. Section 4 presents the results of the experimental validation in a comprehensive manner. Section 5 is the conclusion.

Table 1

Characteristics of existing SOC estimation methods.

Primary type	Secondary type	Method	Accumulated error	Initial SOC dependence	Estimation accuracy	Complexity	Practicability
Defined method	-	AhI [4,5]	Yes	Yes	Medium	Low	Medium
	Linear model	OCV [6]	No	No	Low	Low	Low
		SVM [8], GPR [9], BPNN [10], RBFNN [11], RNN [12,13], LSTM [14–17], GRU [18–21], AE-LSTM [22], DAE-GRU [23]	No	No	Medium	Medium	High
Direct method	ML model	EM-UKF [24], PBM-ACKF [25] P2D-DEKF [26]	Solvable	Solvable	Medium	High	Low
		IFO-EKF [28], FO-ACDFK [29], TM-UKF [30], DP-AHIF [31], TM-IHIF [32], DP-APP [33], TORC-FNTSMO [34]	Solvable	Solvable	Medium	High	Medium
Indirect method		SFNN-EKF [35], FFNN-EKF [36], LSTM-ISRCKF [37]	Solvable	Solvable	Medium	High	Medium
	SOC correction based on ML model	NN-UKF [38], LSTM-UKF [39], LSTM-ACKF [40], LSTM-AHIF [41], IBGRU-UKF [42], LSSVM-UPF [43], Transformer-II0 [44]	Solvable	Solvable	High	High	High
Calibration method	-	DNN-KF [45], DNN [46]	No	No	High	High	High

2. The proposed SOC estimation method

2.1. EI-LSTM with sliding window average voltage input

As the traditional RNN is prone to the disappearance of the error gradient due to too long input sequences in the back propagation process of model training, resulting in the network cannot capture the long-term dependencies. Therefore, the improved RNN using LSTM blocks capable of storing information intelligently can effectively solve the gradient disappearance problem in the traditional RNN. In the field of battery SOC estimation, the LSTM-RNN based method has been widely studied in many articles. However, due to the highly nonlinear dynamic response of the battery, most of the existing networks cannot identify the accurate mapping relation between the battery measured variables (voltage, current and temperature) and SOC when the battery operating voltage and current change drastically, resulting in the significant fluctuations in SOC estimation. The reason is that the battery voltage and current are all real-time sampling data and time-varying information as the input of the network. As a result, when the data in the training dataset changes rapidly, the network can only learn the correspondence between the input data sequence and the output label, but not the non-linear mapping based on the battery internal characteristics. Ultimately, the network only performs well on the training dataset, but poor performance on the unknown dataset, lacking generalization ability.

To address this issue, we introduce an additional slow time-varying information, the average voltage, as the fourth input variable in addition to the real-time measured voltage, current and temperature, which can represent the information similar to the battery OCV to some extent. The average voltage is added to give the network input

information a slow time-varying characteristic, which helps to learn the mapping related to the internal characteristics of battery when the battery voltage and current change drastically, and reduces the fluctuations of the output SOC. Specifically, we adopt the sliding average filtering technology to average the voltage in a window time before the current moment as the sliding window average voltage corresponding at this moment. The specific calculation formula is as follows:

$$AV_t = \frac{1}{m}(V_t + V_{t-1} + \dots + V_{t-(m-1)}), \quad (1)$$

where AV_t is the sliding window average voltage at time t , while V_t is the battery voltage, and m is the size of the sliding window.

After adding the sliding window average voltage to the input of LSTM-RNN, the framework of the SOC estimation using the EI-LSTM with four input variables at time t is shown in Fig. 1, and the forward calculation process is as follows:

$$\begin{cases} f_t = \sigma(U_f \cdot h_{t-1} + W_f \cdot x_t + b_f), \\ i_t = \sigma(U_i \cdot h_{t-1} + W_i \cdot x_t + b_i), \\ o_t = \sigma(U_o \cdot h_{t-1} + W_o \cdot x_t + b_o), \\ \tilde{c}_t = \tanh(U_c \cdot h_{t-1} + W_c \cdot x_t + b_c), \\ c_t = f_t \odot c_{t-1} + i_t \odot \tilde{c}_t, \\ h_t = o_t \odot \tanh c_t, \\ soc_t = g(h_t) = g(V \cdot h_t + b_{soc}), \end{cases} \quad (2)$$

where f_t , i_t and o_t are the forget gate, the input gate and the output gate, respectively. \tilde{c}_t is the candidate state while c_t is the internal state. h_t is the hidden layer state. Logistic sigmoid function $\sigma \in [0, 1]^D$ and hyperbolic tangent function $\tanh \in [-1, 1]^D$. x_t is the four-dimensional

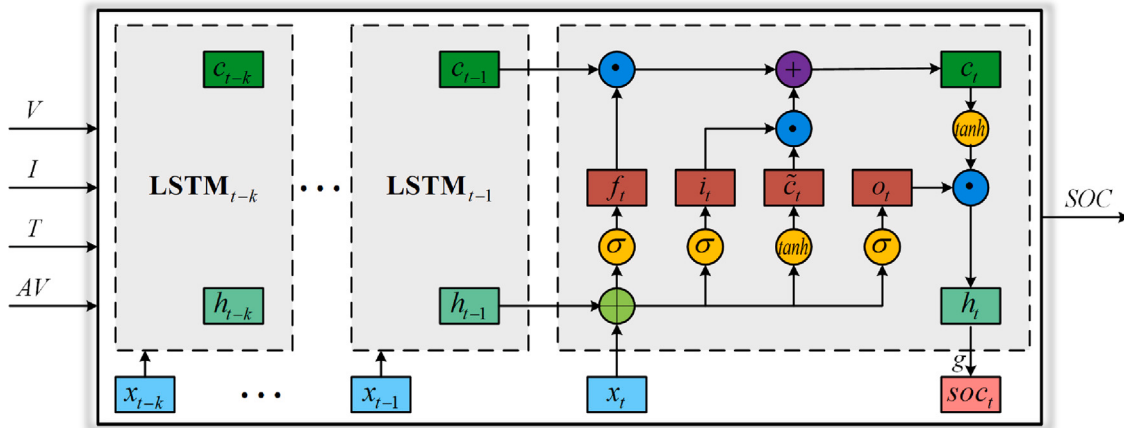


Fig. 1. Framework of the SOC estimation using the EI-LSTM.

Table 2
Hyperparameter settings of the EI-LSTM.

Type	Hyperparameter	Value
Network structure	Number of hidden layers	1
	Number of hidden layer neurons	30
Data structure	Time step	50
	Sliding window size	50
	Data sampling interval	1s
	Normalization range of input data	[-1,1]
	Activation function of output layer	Sigmoid
Training process	Initial network parameters	Random
	Optimizer	Adam
	Initial learning rate	0.01
	Mini-batch size	64
	Training epoch	150
	Loss function	MSE

input vector formed by the battery voltage, current, temperature and average voltage. soc_t is the estimated SOC corresponding to time t . $g(\cdot)$ is the nonlinear activation function of the output layer. U , W and V are the weight matrices. b is the bias vector. \odot denotes the product of the elements between the vectors.

The hyperparameters of the network are set as shown in **Table 2**. As a large number of literatures have proved that the NN with single hidden layer is sufficient for battery SOC prediction [38–41], thus a single hidden layer network with 30 neurons is adopted in this paper. Theoretically, the larger the time step is, the better the mapping ability of the network, but considering the amount of computation, it needs to be set to a moderate size, which is set to 50 in this paper. The sliding window size is an important parameter, which directly affects the degree of the slow time-varying of average voltage, and we finally set it to 50 by testing the results under different sliding window sizes. In the training process, we chose the commonly used mean square error (MSE) as the loss function with the following equation:

$$\text{MSE} = \frac{1}{n} \sum_{i=1}^n (soc_i - \hat{soc}_i)^2, \quad (3)$$

where n is the size of mini-batch. soc_i is the true value of SOC from the Coulomb counting method. \hat{soc}_i is the estimated value from the forward calculation performed by EI-LSTM during training.

2.2. AhI-based output SOC constraint strategy

Since the forward calculation process of each estimation for battery SOC using the LSTM-RNN based method is independent, it leads to the possibility of a relatively large gap between the output SOCs of adjacent moments of the network. However, the battery SOC at adjacent moments should be constrained by the real charge change,

that is, the change direction of the battery SOC at adjacent moments should match the change direction of the current, and the variation of SOC at adjacent moments should not exceed that calculated by the AhI method. Based on this, we propose an AhI-based state flow strategy to constrain the output SOC variation of EI-LSTM at adjacent moments, and the SOC predicted by the EI-LSTM at each moment is input into the constraint strategy for processing to obtain the final estimated SOC, which achieves the effect of smoothing the output SOC of the network.

The specific workflow of the constraint strategy is shown in **Fig. 2**. Where Δt is the data sampling interval, C is the nominal capacity of battery, λ is the constraint factor representing the constraint ability, I_t is the sampling current at time t , discharge is negative and charge is positive, SOC_t^L is the output SOC of the EI-LSTM at time t while SOC_t is the final estimated SOC. Before applying the constraint strategy, we need to initialize the parameters of the AhI method, such as Δt , C and λ . When estimating the SOC, we first input the sampling current I_t and the SOC_t^L predicted by the EI-LSTM at the current moment, and then judge whether the current moment is the initial moment of SOC estimation. If the judgment result is YES, the SOC_t^L is output directly without constraint. This is because there is no adjacent moment output SOC corresponding to the initial moment, so the SOC predicted by the EI-LSTM at the initial moment is the final SOC. If the result is NO, then the next judgment condition is proceeded. In the second judgment condition, we determine whether the change direction of SOC_t^L is the same as that of I_t . The reason is that SOC_t^L should be greater than SOC_{t-1}^L when charging and less than SOC_{t-1}^L when discharging. If the judgment result is NO, the SOC_t^L at this moment is invalid prediction, and the SOC_t at this moment is directly equal to the SOC_{t-1} at the previous moment. If the result is YES, then the next judgment condition is entered. In the third judgment condition, we judge whether the variation between the SOC_t^L at the current moment and the estimated

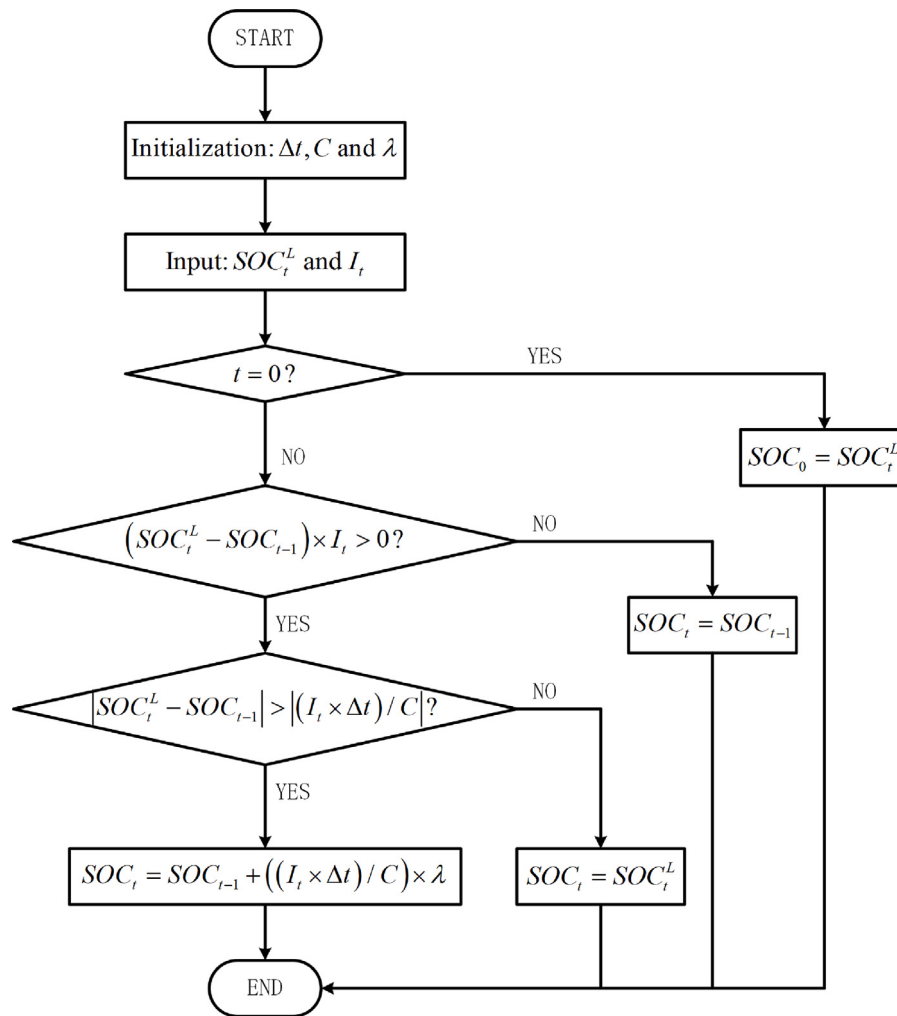


Fig. 2. Flow chart of the AhI-based output SOC constraint strategy.

SOC_{t-1} at the previous moment is greater than the SOC variation calculated by the AhI method in this time period. If the judgment result is NO, the SOC_t^L at this moment is a valid prediction and does not touch the threshold of the SOC variation constrained by the AhI method, then the estimated SOC_t at the current moment is equal to the output SOC_t^L of the EI-LSTM. If the result is YES, it means that the SOC_t^L at this moment touches the threshold of the SOC variation constrained by the AhI method, and then the SOC_t will be obtained by the AhI with constraint factor. In this way, the final estimated SOC at each moment is cyclically calculated.

The constraint factor λ should theoretically be set to 1. However, in our experiments, we found that the output SOC variation of EI-LSTM is much higher than that of AhI method, which is due to the fact that there is always deviation in the mapping between the battery measured variables and SOC learned by the EI-LSTM, especially when the current changes rapidly. When λ is set to 1, the convergence rate of SOC correction by constraint strategy may be too slow when the output SOC of EI-LSTM changes sharply, thus affecting the smoothing performance. Therefore, in order to achieve better constraint effect, it is necessary to increase the value of λ appropriately according to the actual situation, so the λ is set to 1.5 in this paper.

Fig. 3 illustrates the framework of the proposed method EI-LSTM-CO for estimating battery SOC in this paper. The measured data sequence containing battery voltage, current, temperature and average voltage is input into the EI-LSTM to directly map a predicted SOC. And then the predictive SOC is input into the AhI-based state flow constraint

strategy module for smoothing, resulting in the final accurate and stable estimated SOC.

3. Dataset and evaluation criteria

The actual driving conditions of the EV are complex and uncertain. In order to simulate the EV battery load conditions as realistically as possible, this paper uses the dynamic stress testing (DST), US06 driving schedule and the federal urban driving schedule (FUDS) designed by the United States Advanced Battery Consortium (USABC) to simulate the EV driving conditions. Since the DST is a simplification of the actual battery load and considers regenerative charging, the data collected by the DST profile is used as the training dataset for the proposed method in this paper. In order to validate the generalization ability of the SOC estimation method, which means the SOC estimation performance on unknown data, thus the dataset used to test the proposed method should be different from the training dataset. As US06 simulates highway driving conditions and FUDS simulates urban road driving conditions, the data collected by US06 and FUDS profiles are used as unknown test datasets for testing the SOC estimation performance of the proposed method.

In the experiments, we use a public dataset of LiFePO₄ battery from the Center for Advanced Life Cycle Engineering (CALCE) at the University of Maryland [6]. Although this dataset has data on the operating condition at negative temperature, the battery dynamic characteristics are very unstable under negative temperature, which will

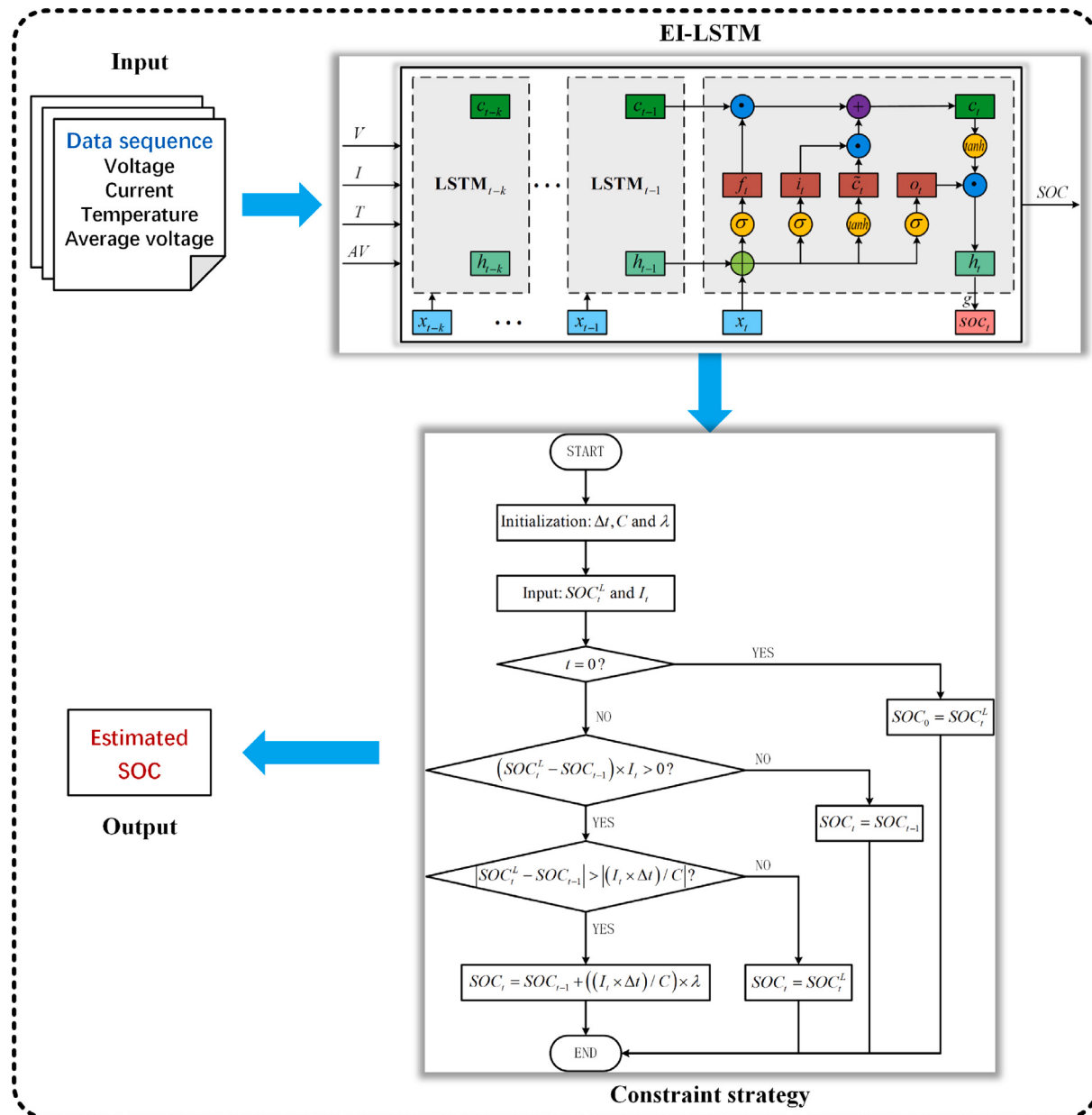


Fig. 3. Framework of the SOC estimation using the proposed method EI-LSTM-CO.

greatly increase the difficulty of SOC estimation and affect the service life of battery, especially for the LiFePO₄ battery. In fact, the existing thermal management technology has been applied more maturely, and it should be recommended to heat the battery to above 0 °C before charging and discharging, which is helpful to improve the accuracy of SOC estimation algorithm and protect the health of battery. Therefore, the DST, US06 and FUDS battery datasets adopted in this paper are all counted at seven different positive temperatures such as 0 °C, 10 °C, 20 °C, 25 °C, 30 °C, 40 °C and 50 °C with a sampling time of 1 s. The current, voltage and temperature profiles of the DST, US06 and FUDS datasets at 25 °C are shown in Fig. 4.

In order to improve the training efficiency and robustness of the network, the battery measured data (voltage, current, temperature and average voltage) need to be properly normalized. Since the network in this paper has both the sigmoid function with an output range of [0, 1] and the tanh function with an output range of [-1, 1], we adopt the minimum–maximum normalization to map the battery measured data of the above three datasets to the interval of [-1, 1]. The equation is

as follows.

$$x_{norm} = \frac{2(x_{orig} - x_{min})}{x_{max} - x_{min}} - 1, \quad (4)$$

where \$x_{max}\$ and \$x_{min}\$ are the maximum and minimum values of the measured variables in the dataset respectively. \$x_{orig}\$ is the original value. And \$x_{norm}\$ is the corresponding normalized value, which is the actual input data of the network.

In this paper, two different error functions are used to evaluate the SOC estimation performance of the proposed method, namely the root mean square error (RMSE) and the maximum error (MAXE), which are defined as follows:

$$RMSE = \sqrt{\frac{1}{N} \sum_{i=1}^N (soc_i - \hat{soc}_i)^2}, \quad (5)$$

$$MAXE = \max(|soc_i - \hat{soc}_i|), 1 \leq i \leq N, \quad (6)$$

where \$N\$ is the total number of samples. \$soc_i\$ is the true value of SOC from the Coulomb counting method while \$\hat{soc}_i\$ is the estimated value

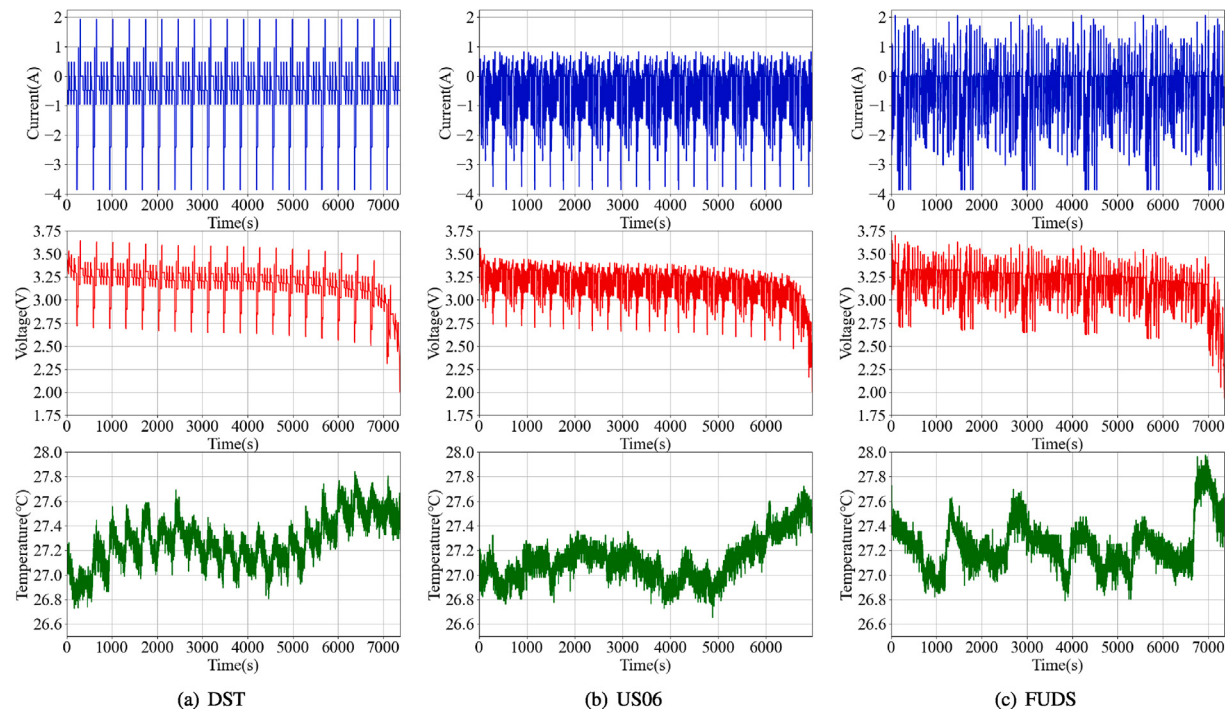


Fig. 4. Current, voltage and temperature profiles of the DST, US06 and FUDS at 25 °C.

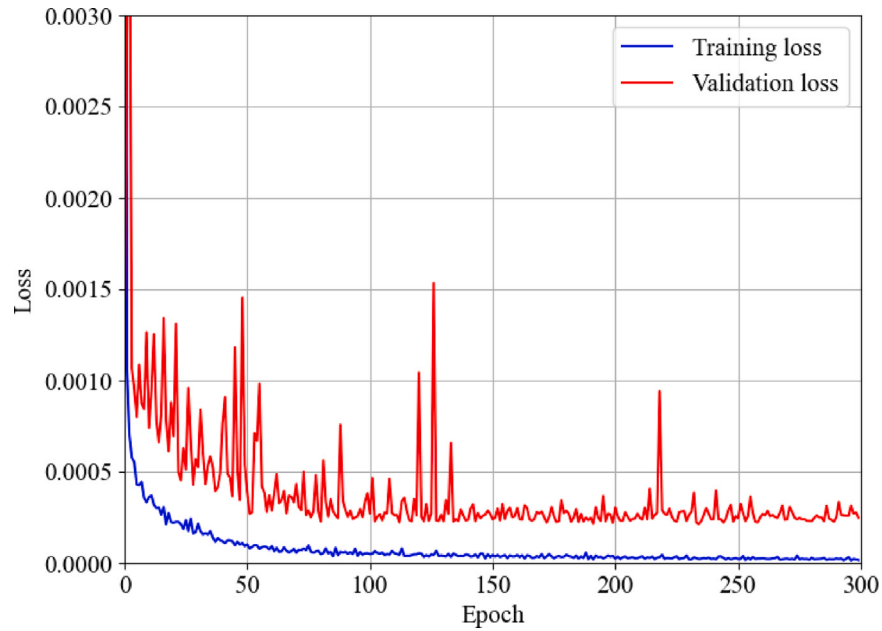


Fig. 5. Training loss and validation loss of the EI-LSTM.

from the SOC estimation method. The RMSE indicates the robustness of the estimation and the MAXE indicates the extreme results.

4. Experimental results

4.1. SOC estimation using EI-LSTM

This subsection performs the validation of the SOC estimation performance of the EI-LSTM with the addition of sliding window average voltage input. Firstly, the EI-LSTM is trained using the DST dataset within the full temperature range according to the setting of hyperparameters in Table 2. Meanwhile, for observing the generalization ability

of the network during training, we use the US06 and FUDS datasets as validation datasets and record the training loss and validation loss for each training epoch, as shown in Fig. 5. Since the validation dataset is completely different from the training dataset, we can see that the validation loss is significantly higher than the training loss. Furthermore, it can be seen from the figure that the validation loss of the network almost stops decreasing from the 150th epoch, and there is a slight increase thereafter, which indicates the appearance of overfitting. Therefore, we choose the network at the 150th epoch as the final experimental model in this paper. In addition, we also perform the same training on the LSTM-RNN without average voltage input, and by comparing the estimation errors of the LSTM-RNN and the EI-LSTM, the

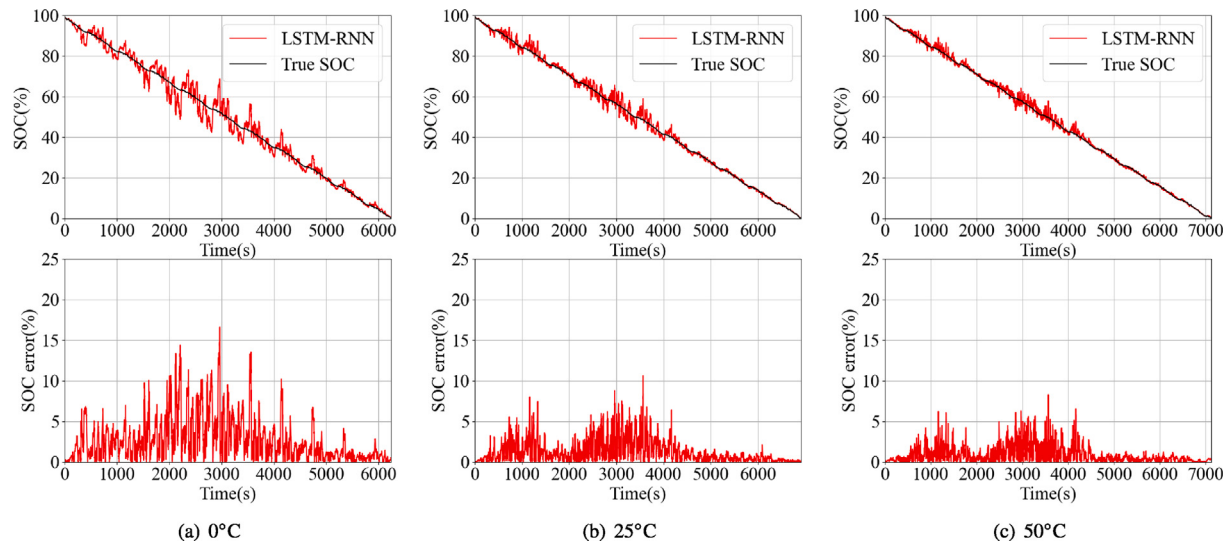


Fig. 6. SOC estimation results of the LSTM-RNN for US06 at different temperatures.

Table 3

Comparison results of SOC estimation for US06 and FUDS using the LSTM-RNN, the EI-LSTM and the EI-LSTM-CO.

Dataset	Temperature (°C)	LSTM-RNN		EI-LSTM		EI-LSTM-CO	
		RMSE (%)	MAXE (%)	RMSE (%)	MAXE (%)	RMSE (%)	MAXE (%)
US06	0	3.7	16.6	2.4	9.6	1.3	3.1
	10	2.9	11.5	2.0	7.3	1.3	3.2
	20	2.0	8.5	1.1	5.2	0.5	1.6
	25	1.8	10.6	1.0	4.2	0.4	1.3
	30	1.7	8.5	1.0	3.7	0.4	1.4
	40	1.4	10.7	1.0	4.5	0.5	1.5
	50	1.3	8.3	0.9	5.3	0.4	1.2
FUDS	0	3.8	15.5	3.1	15.3	1.5	2.8
	10	3.3	13.9	1.8	10.1	0.8	2.9
	20	2.3	12.1	1.4	7.6	0.7	2.8
	25	2.3	11.5	1.2	6.8	0.5	2.3
	30	2.1	11.0	1.3	7.1	0.6	1.6
	40	1.6	9.2	1.3	5.9	0.7	2.0
	50	1.4	8.4	1.3	6.8	0.8	2.1

effectiveness of adding the sliding window average voltage to improve the SOC estimation performance can be validated.

Next, we validate the SOC estimation performance of the trained LSTM-RNN and EI-LSTM at different temperatures by using unknown datasets US06 and FUDS, which are different from the training dataset. Figs. 6, 7, 8 and 9 show the SOC estimation results and the corresponding estimation errors for the above two networks using the US06 and FUDS datasets at 0 °C, 25 °C and 50 °C respectively. The SOC estimation results at all temperatures are tabulated in Table 3, and the true SOC is calculated by the Coulomb counting method. It can be seen from the figures that both networks can capture the downturn of SOC on the unknown data at different temperatures, which proves that they have the generalization ability for different driving conditions and temperatures. However, by comparing Figs. 6 and 7 with Figs. 8 and 9, it can be found that the output SOC fluctuations of EI-LSTM is obviously lower than that of LSTM-RNN, especially the fluctuations are significantly weakened when the voltage and current change sharply. As shown in Table 3, compared with the LSTM-RNN, the RMSE of estimated SOC of EI-LSTM is lower, which indicates that the SOC estimation performance of EI-LSTM is better than that of LSTM-RNN at different temperatures. This proves that adding average voltage to the network input information can reduce the network output SOC fluctuations and improving the estimation performance.

4.2. SOC estimation after constraining

In the previous subsection, we reduce the fluctuations of the network output SOC by adding additional input information to the conventional LSTM-RNN. However, the RMSE of the network output SOC is still as high as 3.1%, and especially the MAXE is still up to 15.5%. Therefore, in order to meet the requirements of practical application, the accuracy and stability of the network estimated SOC need to be further improved. In this subsection, the Ahl-based constraint strategy is used to further smooth the output SOC of the EI-LSTM and improve the accuracy and stability of SOC estimation. Figs. 10 and 11 are the results after smoothing the output SOC of EI-LSTM using the proposed constraint strategy under US06 and FUDS datasets respectively, and the SOC estimation results after constraining at all temperatures are shown in Table 3. By comparing Figs. 8 and 9 with Figs. 10 and 11, it can be seen that adding the constraint strategy can greatly smooth out the fluctuations of the original output from the EI-LSTM and make the final estimated SOC smooth. Table 3 summarizes the comparison of the SOC estimation performance using the EI-LSTM and the EI-LSTM-CO. The results show that adding the constraint strategy to the output SOC of EI-LSTM can further reduce the error of SOC estimation. In particular, the RMSE is reduced from 3.1% to 1.3% and the MAXE is

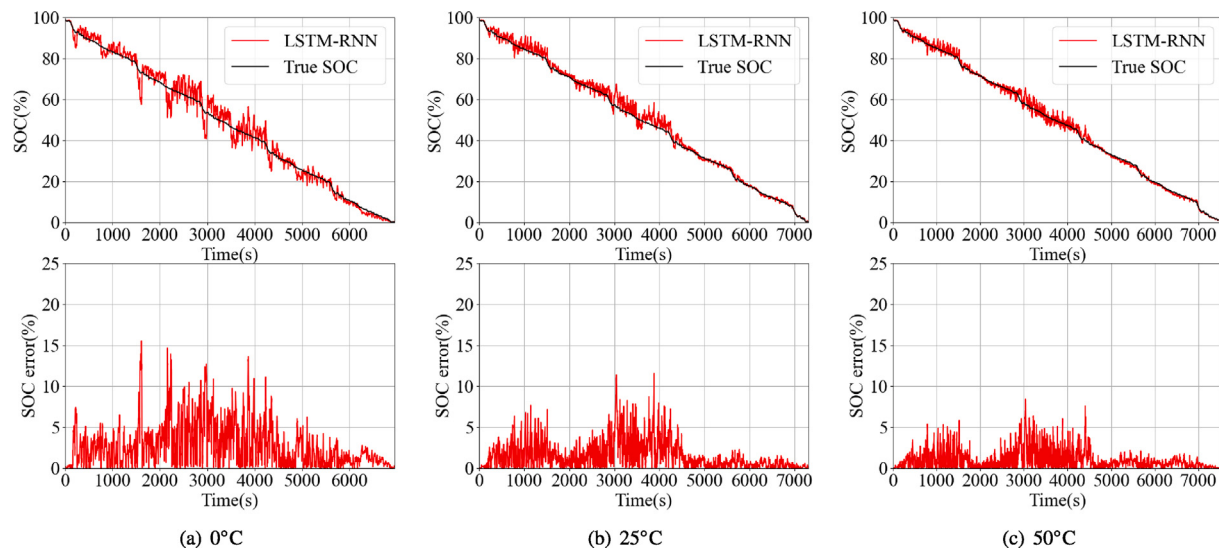


Fig. 7. SOC estimation results of the LSTM-RNN for FUDS at different temperatures.

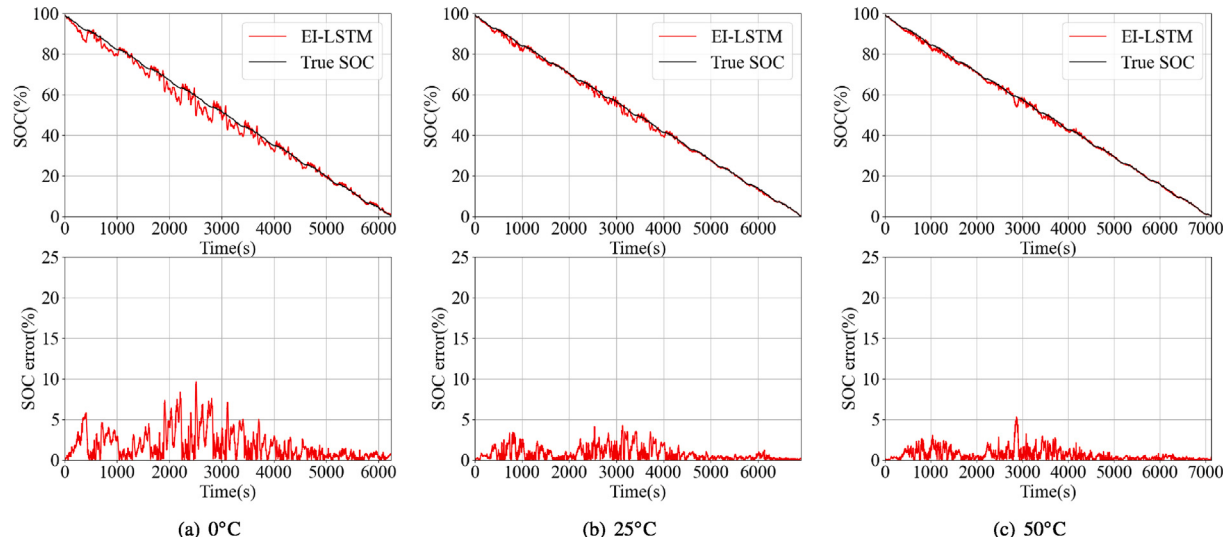


Fig. 8. SOC estimation results of the EI-LSTM for US06 at different temperatures.

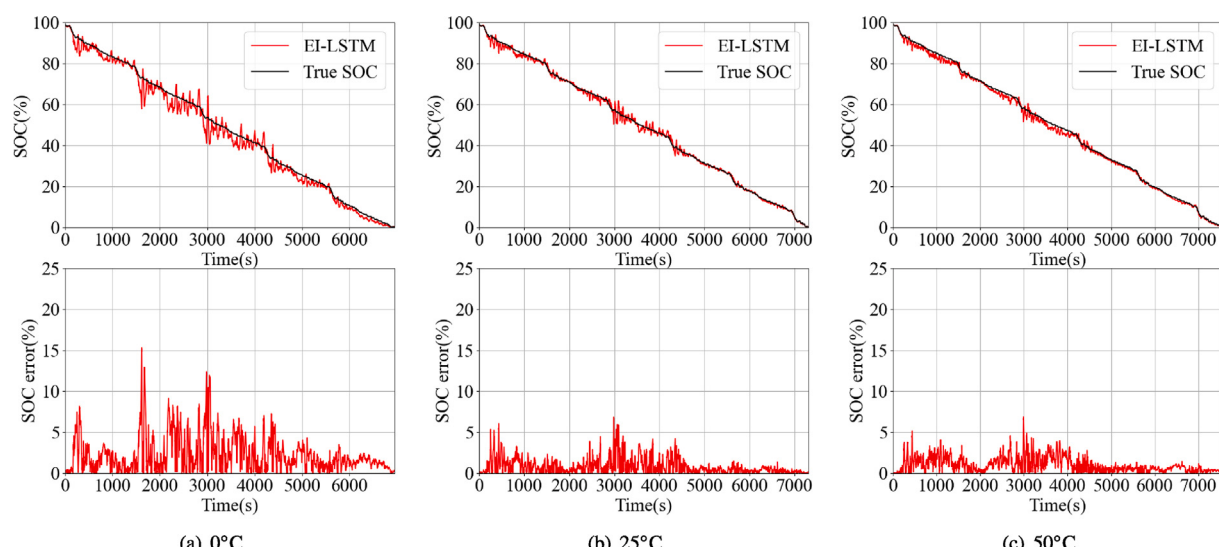


Fig. 9. SOC estimation results of the EI-LSTM for FUDS at different temperatures.

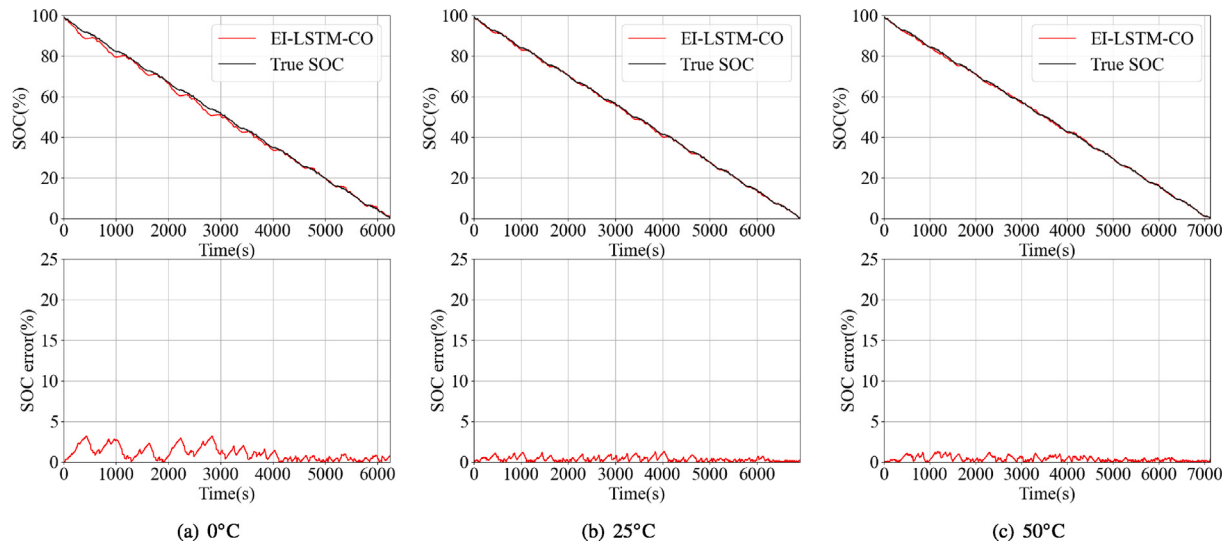


Fig. 10. SOC estimation results of the EI-LSTM-CO for US06 at different temperatures.

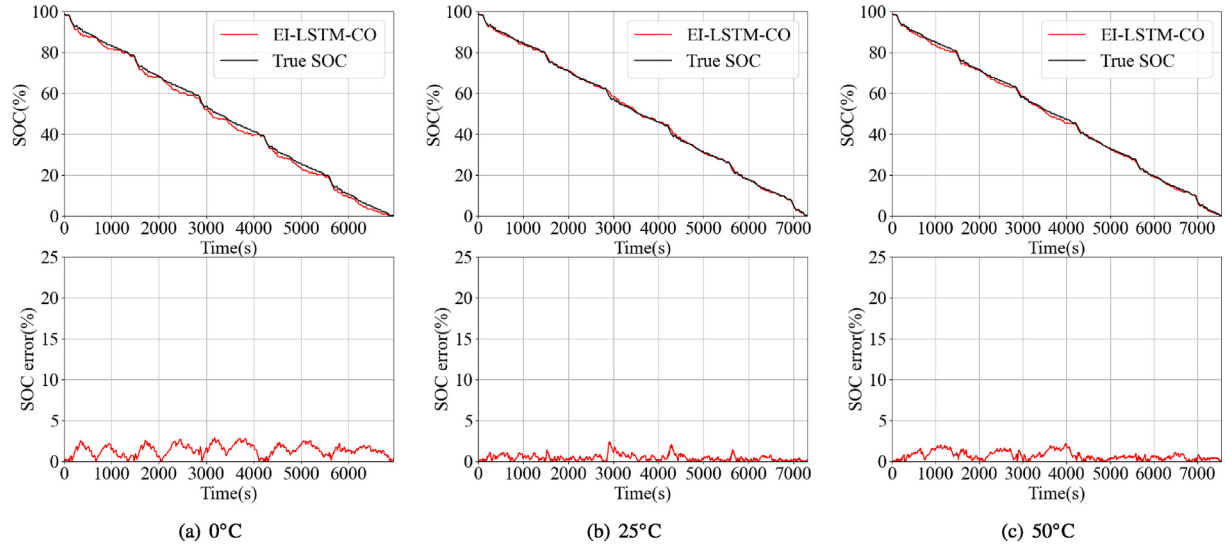


Fig. 11. SOC estimation results of the EI-LSTM-CO for FUDS at different temperatures.

from 15.5% to 3.2%. In conclusion, adding the SOC constraint strategy to the output of the conventional LSTM-RNN is an effective way to improve the accuracy and stability of the network estimated SOC.

4.3. Comparison of the proposed method with other methods

To demonstrate the superiority of the proposed method in battery SOC estimation performance, we compare the experimental results of EI-LSTM-CO with that of other methods. And in order to make a more rigorous comparison, we select the methods using the same training and test datasets to compare with EI-LSTM-CO. Specifically, these methods are all trained using the DST datasets at different temperatures from the public dataset of CALCE and tested using the US06 and FUDS datasets. The comparison results are shown in Table 4. It can be seen that the RMSE of EI-LSTM-CO on the unknown operating conditions at different temperatures is more lower than that of the other two methods, indicating that the EI-LSTM-CO has better robustness for SOC estimation. However, in terms of the MAXE, the performance of the EI-LSTM-CO is inferior to the NN-UKF [38], but better than the LSTM-ACKF [40]. Although the superiority of the MAXE is not as good as the

RMSE for the EI-LSTM-CO, its overall performance is better than the other two methods. Actually, the proposed EI-LSTM-CO in this paper is not like the other two methods which take the AhI method as the main calculation part, so it is not as good as NN-UKF in dealing with the peak estimation, but its MAXE has been fully satisfied for practical applications. In addition, to highlight the excellent computation efficiency of the proposed output SOC smoothing method, a comparison about the single calculation time of the UKF and ACKF in other two methods with the proposed AhI-based constraint strategy is designed on the experimental machine (CPU: Intel i7-10700K @3.80 GHz, GPU: NVIDIA GeForce RTX 3080, Memory: 16 GB, OS: Win10 x64), and the results are shown in Table 5. Obviously, the proposed AhI-based state flow constraint strategy has faster computing speed due to its simpler framework than the filtering algorithm, which is the major advantage of EI-LSTM-CO. Therefore, the comparison results prove that the proposed EI-LSTM-CO has superior SOC estimation performance and meets the requirements of engineering application. In addition, since the SOC estimation method proposed in this paper is a direct mapping, which is different from the iterative calculation process based on the AhI method, thus the BMS does not need to set an accurate

Table 4

Comparison of the proposed EI-LSTM-CO with other methods in SOC estimation errors for US06 and FUDS at different temperatures.

Dataset	Temperature (°C)	RMSE (%)			MAXE (%)		
		NN-UKF [38]	LSTM-ACKF [40]	EI-LSTM-CO	NN-UKF [38]	LSTM-ACKF [40]	EI-LSTM-CO
US06	0	2.4	—	1.3	3.4	—	3.1
	10	2.1	0.8	1.3	2.7	2.2	3.2
	20	0.9	—	0.5	1.3	—	1.6
	25	2.5	1.0	0.4	3.5	1.8	1.3
	30	1.3	0.9	0.4	1.9	1.7	1.4
	40	1.0	1.2	0.5	1.5	2.7	1.5
	50	1.0	1.2	0.4	1.3	2.5	1.2
FUDS	0	2.2	—	1.5	3.1	—	2.8
	10	0.5	1.6	0.8	1.4	3.5	2.9
	20	0.5	—	0.7	1.6	—	2.8
	25	1.4	0.9	0.5	1.9	2.7	2.3
	30	0.9	1.2	0.6	1.3	2.9	1.6
	40	0.6	1.8	0.7	1.0	3.2	2.0
	50	1.0	2.2	0.8	1.4	3.8	2.1

Table 5

Comparison of the proposed AhI-based constraint strategy with other smoothing methods in computation efficiency.

Smoothing method	UKF [38]	ACKF [40]	AhI-based constraint strategy
Computation time (ms)	0.0124	0.0608	0.0035

initial value to start the SOC estimation process. Therefore, there is no experiment to validate the convergence rate of initial SOC in this paper.

5. Conclusions

By extending the network input and constraining the network output, this paper proposes a novel LSTM-RNN-based battery SOC estimation method, named EI-LSTM-CO. And then the SOC estimation performance and generalization ability of the proposed method are validated using a public dataset of LiFePO₄ battery. The experimental results show that adding the sliding window average voltage to the input variables of the conventional LSTM-RNN which only uses the fast time-varying input information such as battery measured voltage, current, and temperature can help the network to learn the mapping related to the internal characteristics of the battery better and reduce the fluctuations in the network output SOC. On this basis, an AhI-based state flow constraint strategy is designed at the output of the EI-LSTM, and the experimental results demonstrate that the constraint strategy can further stabilize the network output SOC and greatly improve the estimation accuracy. Specifically, the RMSE and MAXE of the proposed EI-LSTM-CO on the unknown data at different temperatures are below 1.3% and 3.2% respectively, with satisfactory SOC estimation performance and generalization ability. The comparative experiments with other existing methods using the same dataset demonstrate the superiority of the proposed method in SOC estimation.

Compared with the existing ML model-based methods, as the output SOC of EI-LSTM will be further processed by the AhI-based constraint strategy, so we do not need to design the hyperparameters of network carefully, which reduces the time-consuming of the estimator design. In contrast to the ML model-based SOC correction method which takes the AhI method as the main calculation part, the proposed AhI-based constraint strategy in this paper is designed to play the role of assisting LSTM-RNN to estimate SOC stably, thus it does not change the essence of the proposed method belonging to the ML model method, so there is no dependence problem on the initial SOC. Moreover, the AhI-based constraint strategy has a simpler structure than the filter or observer on the premise of ensuring the SOC smoothing performance of network output, and so the proposed method has greater engineering application value.

CRediT authorship contribution statement

Junxiong Chen: Investigation, Conceptualization, Methodology. **Yu Zhang:** Software, Validation, Data curation. **Ji Wu:** Writing – original draft. **Weisong Cheng:** Writing – review & editing. **Qiao Zhu:** Supervision.

Declaration of competing interest

The authors declare that they have no known competing financial interests or personal relationships that could have appeared to influence the work reported in this paper.

Data availability

The authors do not have permission to share data.

Acknowledgments

We would like to acknowledge the grant from National Natural Science Foundation of China, China, Grant number 51775450 and grant from Sichuan Science and Technology Program, China, grant number 2022YFG0094 and 2019JDRC0025.

References

- [1] Luo K, Chen X, Zheng H, Shi Z. A review of deep learning approach to predicting the state of health and state of charge of lithium-ion batteries. *J Energy Chem* 2022;74:159–73. <http://dx.doi.org/10.1016/j.jecchem.2022.06.049>, URL: <https://www.sciencedirect.com/science/article/pii/S2095495622003564>.
- [2] Yang B, Wang J, Cao P, Zhu T, Shu H, Chen J, Zhang J, Zhu J. Classification, summarization and perspectives on state-of-charge estimation of lithium-ion batteries used in electric vehicles: A critical comprehensive survey. *J Energy Storage* 2021;39:102572. <http://dx.doi.org/10.1016/j.est.2021.102572>, URL: <https://www.sciencedirect.com/science/article/pii/S2352152X21003170>.
- [3] Wang Y, Tian J, Sun Z, Wang L, Xu R, Li M, Chen Z. A comprehensive review of battery modeling and state estimation approaches for advanced battery management systems. *Renew Sustain Energy Rev* 2020;131:110015. <http://dx.doi.org/10.1016/j.rser.2020.110015>, URL: <https://www.sciencedirect.com/science/article/pii/S1364032120303063>.
- [4] Ng KS, Moo C-S, Chen Y-P, Hsieh Y-C. Enhanced coulomb counting method for estimating state-of-charge and state-of-health of lithium-ion batteries. *Appl Energy* 2009;86(9):1506–11. <http://dx.doi.org/10.1016/j.apenergy.2008.11.021>, URL: <https://www.sciencedirect.com/science/article/pii/S0306261908003061>.
- [5] Zhang S, Guo X, Dou X, Zhang X. A data-driven coulomb counting method for state of charge calibration and estimation of lithium-ion battery. *Sustain Energy Technol Assess* 2020;40:100752. <http://dx.doi.org/10.1016/j.seta.2020.100752>, URL: <https://www.sciencedirect.com/science/article/pii/S2213138820300527>.

- [6] Xing Y, He W, Pecht M, Tsui KL. State of charge estimation of lithium-ion batteries using the open-circuit voltage at various ambient temperatures. *Appl Energy* 2014;113:106–15. <http://dx.doi.org/10.1016/j.apenergy.2013.07.008>, URL: <https://www.sciencedirect.com/science/article/pii/S0306261913005746>.
- [7] Hossain Lipu M, Hannan M, Hussain A, Ayob A, Saad MH, Karim TF, How DN. Data-driven state of charge estimation of lithium-ion batteries: Algorithms, implementation factors, limitations and future trends. *J Cleaner Prod* 2020;277:124110. <http://dx.doi.org/10.1016/j.jclepro.2020.124110>, URL: <http://www.sciencedirect.com/science/article/pii/S095965262034155X>.
- [8] Manoharan A, Begam K, Aparow VR, Sooriomothy D. Artificial neural networks, gradient boosting and support vector machines for electric vehicle battery state estimation: A review. *J Energy Storage* 2022;55:105384. <http://dx.doi.org/10.1016/j.est.2022.105384>, URL: <https://www.sciencedirect.com/science/article/pii/S2352152X22013780>.
- [9] Babaeiyazdi I, Rezaei-Zare A, Shokrzadeh S. State of charge prediction of EV Li-ion batteries using EIS: A machine learning approach. *Energy* 2021;223:120116. <http://dx.doi.org/10.1016/j.energy.2021.120116>, URL: <https://www.sciencedirect.com/science/article/pii/S0360544221003650>.
- [10] Mao X, Song S, Ding F. Optimal BP neural network algorithm for state of charge estimation of lithium-ion battery using PSO with Levy flight. *J Energy Storage* 2022;49:104139. <http://dx.doi.org/10.1016/j.est.2022.104139>, URL: <https://www.sciencedirect.com/science/article/pii/S2352152X22001736>.
- [11] Zhang G, Xia B, Wang J, Ye B, Chen Y, Yu Z, Li Y. Intelligent state of charge estimation of battery pack based on particle swarm optimization algorithm improved radical basis function neural network. *J Energy Storage* 2022;50:104211. <http://dx.doi.org/10.1016/j.est.2022.104211>, URL: <https://www.sciencedirect.com/science/article/pii/S2352152X22002420>.
- [12] Feng X, Chen J, Zhang Z, Miao S, Zhu Q. State-of-charge estimation of lithium-ion battery based on clockwork recurrent neural network. *Energy* 2021;236:121360. <http://dx.doi.org/10.1016/j.energy.2021.121360>, URL: <https://www.sciencedirect.com/science/article/pii/S036054422101608X>.
- [13] Xi Z, Wang R, Fu Y, Mi C. Accurate and reliable state of charge estimation of lithium ion batteries using time-delayed recurrent neural networks through the identification of overexcited neurons. *Appl Energy* 2022;305:117962. <http://dx.doi.org/10.1016/j.apenergy.2021.117962>, URL: <https://www.sciencedirect.com/science/article/pii/S0306261921012691>.
- [14] Ren X, Liu S, Yu X, Dong X. A method for state-of-charge estimation of lithium-ion batteries based on PSO-LSTM. *Energy* 2021;234:121236. <http://dx.doi.org/10.1016/j.energy.2021.121236>, URL: <https://www.sciencedirect.com/science/article/pii/S0360544221014845>.
- [15] Ma L, Hu C, Cheng F. State of charge and state of energy estimation for lithium-ion batteries based on a long short-term memory neural network. *J Energy Storage* 2021;37:102440. <http://dx.doi.org/10.1016/j.est.2021.102440>, URL: <https://www.sciencedirect.com/science/article/pii/S2352152X21001924>.
- [16] Almaita E, Alshkoor S, Abdelsalam E, Almomani F. State of charge estimation for a group of lithium-ion batteries using long short-term memory neural network. *J Energy Storage* 2022;52:104761. <http://dx.doi.org/10.1016/j.est.2022.104761>, URL: <https://www.sciencedirect.com/science/article/pii/S2352152X2200771X>.
- [17] Oyewole I, Chehade A, Kim Y. A controllable deep transfer learning network with multiple domain adaptation for battery state-of-charge estimation. *Appl Energy* 2022;312:118726. <http://dx.doi.org/10.1016/j.apenergy.2022.118726>, URL: <https://www.sciencedirect.com/science/article/pii/S0306261922001842>.
- [18] Jiao M, Wang D, Qiu J. A GRU-RNN based momentum optimized algorithm for SOC estimation. *J Power Sources* 2020;459:228051. <http://dx.doi.org/10.1016/j.jpowsour.2020.228051>, URL: <https://www.sciencedirect.com/science/article/pii/S0378775320303542>.
- [19] Xiao F, Li C, Fan Y, Yang G, Tang X. State of charge estimation for lithium-ion battery based on Gaussian process regression with deep recurrent kernel. *Int J Electr Power Energy Syst* 2021;124:106369. <http://dx.doi.org/10.1016/j.ijepes.2020.106369>, URL: <https://www.sciencedirect.com/science/article/pii/S0142061520300247>.
- [20] Yang K, Tang Y, Zhang S, Zhang Z. A deep learning approach to state of charge estimation of lithium-ion batteries based on dual-stage attention mechanism. *Energy* 2022;244:123233. <http://dx.doi.org/10.1016/j.energy.2022.123233>, URL: <https://www.sciencedirect.com/science/article/pii/S0360544222001360>.
- [21] Wang Y-X, Chen Z, Zhang W. Lithium-ion battery state-of-charge estimation for small target sample sets using the improved GRU-based transfer learning. *Energy* 2022;244:123178. <http://dx.doi.org/10.1016/j.energy.2022.123178>, URL: <https://www.sciencedirect.com/science/article/pii/S0360544222000810>.
- [22] Fasahat M, Manthouri M. State of charge estimation of lithium-ion batteries using hybrid autoencoder and long short term memory neural networks. *J Power Sources* 2020;469:228375. <http://dx.doi.org/10.1016/j.jpowsour.2020.228375>, URL: <http://www.sciencedirect.com/science/article/pii/S0378775320306790>.
- [23] Chen J, Feng X, Jiang L, Zhu Q. State of charge estimation of lithium-ion battery using denoising autoencoder and gated recurrent unit recurrent neural network. *Energy* 2021;227:120451. <http://dx.doi.org/10.1016/j.energy.2021.120451>, URL: <https://www.sciencedirect.com/science/article/pii/S0360544221007003>.
- [24] Santhanagopalan S, White RE. State of charge estimation using an unscented filter for high power lithium ion cells. *Int J Energy Res* 2010;34(2):152–63. <http://dx.doi.org/10.1002/er.1655>, URL: <https://onlinelibrary.wiley.com/doi/abs/10.1002/er.1655>.
- [25] Li X, Huang Z, Tian J, Tian Y. State-of-charge estimation tolerant of battery aging based on a physics-based model and an adaptive cubature Kalman filter. *Energy* 2021;220:119767. <http://dx.doi.org/10.1016/j.energy.2021.119767>, URL: <https://www.sciencedirect.com/science/article/pii/S0360544221000165>.
- [26] Gao Y, Liu K, Zhu C, Zhang X, Zhang D. Co-estimation of state-of-charge and state-of-health for lithium-ion batteries using an enhanced electrochemical model. *IEEE Trans Ind Electron* 2022;69(3):2684–96. <http://dx.doi.org/10.1109/TIE.2021.3066946>.
- [27] Hossain M, Haque M, Arif M. Kalman filtering techniques for the online model parameters and state of charge estimation of the Li-ion batteries: A comparative analysis. *J Energy Storage* 2022;51:104174. <http://dx.doi.org/10.1016/j.est.2022.104174>, URL: <https://www.sciencedirect.com/science/article/pii/S2352152X22002067>.
- [28] Solomon OO, Zheng W, Chen J, Qiao Z. State of charge estimation of lithium-ion battery using an improved fractional-order extended Kalman filter. *J Energy Storage* 2022;49:104007. <http://dx.doi.org/10.1016/j.est.2022.104007>, URL: <https://www.sciencedirect.com/science/article/pii/S2352152X22000512>.
- [29] He L, Wang Y, Wei Y, Wang M, Hu X, Shi Q. An adaptive central difference Kalman filter approach for state of charge estimation by fractional order model of lithium-ion battery. *Energy* 2022;244:122627. <http://dx.doi.org/10.1016/j.energy.2021.122627>, URL: <https://www.sciencedirect.com/science/article/pii/S0360544221028760>.
- [30] Feng F, Teng S, Liu K, Xie J, Xie Y, Liu B, Li K. Co-estimation of lithium-ion battery state of charge and state of temperature based on a hybrid electrochemical-thermal-neural-network model. *J Power Sources* 2020;455:227935. <http://dx.doi.org/10.1016/j.jpowsour.2020.227935>, URL: <https://www.sciencedirect.com/science/article/pii/S037877532030238X>.
- [31] Ouyang T, Xu P, Chen J, Su Z, Huang G, Chen N. A novel state of charge estimation method for lithium-ion batteries based on bias compensation. *Energy* 2021;226:120348. <http://dx.doi.org/10.1016/j.energy.2021.120348>, URL: <https://www.sciencedirect.com/science/article/pii/S0360544221005971>.
- [32] Chen Z, Zhou J, Zhou F, Xu S. State-of-charge estimation of lithium-ion batteries based on improved H infinity filter algorithm and its novel equalization method. *J Cleaner Prod* 2021;290:125180. <http://dx.doi.org/10.1016/j.jclepro.2020.125180>, URL: <https://www.sciencedirect.com/science/article/pii/S0959652620352240>.
- [33] Li L, Wang C, Yan S, Zhao W. A combination state of charge estimation method for ternary polymer lithium battery considering temperature influence. *J Power Sources* 2021;484:229204. <http://dx.doi.org/10.1016/j.jpowsour.2020.229204>, URL: <https://www.sciencedirect.com/science/article/pii/S0378775320314932>.
- [34] Rezaei O, Moghadam HA, Papari B. A fast sliding-mode-based estimation of state-of-charge for lithium-ion batteries for electric vehicle applications. *J Energy Storage* 2022;45:103484. <http://dx.doi.org/10.1016/j.est.2021.103484>, URL: <https://www.sciencedirect.com/science/article/pii/S2352152X21011671>.
- [35] Xu L, Wang J, Chen Q. Kalman filtering state of charge estimation for battery management system based on a stochastic fuzzy neural network battery model. *Energy Convers Manage* 2012;53(1):33–9. <http://dx.doi.org/10.1016/j.enconman.2011.06.003>, URL: <https://www.sciencedirect.com/science/article/pii/S0196890411001828>.
- [36] Chen C, Xiong R, Yang R, Shen W, Sun F. State-of-charge estimation of lithium-ion battery using an improved neural network model and extended Kalman filter. *J Cleaner Prod* 2019;234:1153–64. <http://dx.doi.org/10.1016/j.jclepro.2019.06.273>, URL: <https://www.sciencedirect.com/science/article/pii/S0959652619322383>.
- [37] Shu X, Li G, Zhang Y, Shen S, Chen Z, Liu Y. Stage of charge estimation of lithium-ion battery packs based on improved Cubature Kalman filter with long short-term memory model. *IEEE Transp Transp Electrif* 2021;7(3):1271–84. <http://dx.doi.org/10.1109/TTE.2020.3041757>.
- [38] He W, Williard N, Chen C, Pecht M. State of charge estimation for li-ion batteries using neural network modeling and unscented Kalman filter-based error cancellation. *Int J Electr Power Energy Syst* 2014;62:783–91. <http://dx.doi.org/10.1016/j.ijepes.2014.04.059>, URL: <https://www.sciencedirect.com/science/article/pii/S0142061514002646>.
- [39] Yang F, Zhang S, Li W, Miao Q. State-of-charge estimation of lithium-ion batteries using LSTM and UKf. *Energy* 2020;201:117664. <http://dx.doi.org/10.1016/j.energy.2020.117664>, URL: <https://www.sciencedirect.com/science/article/pii/S0360544220307714>.
- [40] Tian Y, Lai R, Li X, Xiang L, Tian J. A combined method for state-of-charge estimation for lithium-ion batteries using a long short-term memory network and an adaptive cubature Kalman filter. *Appl Energy* 2020;265:114789. <http://dx.doi.org/10.1016/j.apenergy.2020.114789>, URL: <https://www.sciencedirect.com/science/article/pii/S0306261920303019>.

- [41] Chen Z, Zhao H, Shu X, Zhang Y, Shen J, Liu Y. Synthetic state of charge estimation for lithium-ion batteries based on long short-term memory network modeling and adaptive H-infinity filter. Energy 2021;228:120630. <http://dx.doi.org/10.1016/j.energy.2021.120630>, URL: <https://www.sciencedirect.com/science/article/pii/S0360544221008793>.
- [42] Cui Z, Kang L, Li L, Wang L, Wang K. A combined state-of-charge estimation method for lithium-ion battery using an improved BGRU network and UKf. Energy 2022;259:124933. <http://dx.doi.org/10.1016/j.energy.2022.124933>, URL: <https://www.sciencedirect.com/science/article/pii/S0360544222018345>.
- [43] Song Y, Liu D, Liao H, Peng Y. A hybrid statistical data-driven method for online joint state estimation of lithium-ion batteries. Appl Energy 2020;261:114408. <http://dx.doi.org/10.1016/j.apenergy.2019.114408>, URL: <https://www.sciencedirect.com/science/article/pii/S0306261919320951>.
- [44] Shen H, Zhou X, Wang Z, Wang J. State of charge estimation for lithium-ion battery using transformer with immersion and invariance adaptive observer. J Energy Storage 2022;45:103768. <http://dx.doi.org/10.1016/j.est.2021.103768>, URL: <https://www.sciencedirect.com/science/article/pii/S2352152X21014419>.
- [45] Tian J, Xiong R, Shen W, Lu J. State-of-charge estimation of LiFePO₄ batteries in electric vehicles: A deep-learning enabled approach. Appl Energy 2021;291:116812. <http://dx.doi.org/10.1016/j.apenergy.2021.116812>, URL: <https://www.sciencedirect.com/science/article/pii/S0306261921003147>.
- [46] Hu C, Ma L, Guo S, Guo G, Han Z. Deep learning enabled state-of-charge estimation of LiFePO₄ batteries: A systematic validation on state-of-the-art charging protocols. Energy 2022;246:123404. <http://dx.doi.org/10.1016/j.energy.2022.123404>, URL: <https://www.sciencedirect.com/science/article/pii/S0360544222003073>.